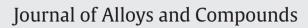
Contents lists available at ScienceDirect







journal homepage: www.elsevier.com/locate/jallcom

Subject Index of Volume 499

Acoustic Debye temperature

thermodynamic properties of Mg_2Si and Mg_2Ge investigated by first principles method 68

Amidoboranes

towards Y(NH₂BH₃)₃: Probing hydrogen storage properties of YX₃/MNH₂BH₃ (X = F, Cl; M = Li, Na) and YH_{x-3}/NH₃BH₃ composites 144

Annealing at different temperature

annealing effects of co-doping with Al and Sb on structure and opticalelectrical properties of the ZnO thin films 265

Ball milling

the mechanochemical stability of hydrogen titanate nanostructures 113 Band gap

preparation and characterization of $Ga_{2x}In_{2(1-x)}O_3$ films deposited on ZrO_2 (1 0 0) substrates by MOCVD 75

Band structures

- first-principles study of the ternary semiconductor alloys (Ga,Al)(As,Sb) 80 Barium strontium titanate
- Sol–gel synthesis and characterization of $Ba_{(1-x)}Sr_xTiO_3$ ceramics 255 Bi: 2212
 - effect of melting time on the superconductivity in Bi_{1.7}Pb_{0.3}Sr₂CaCu₂O₈ superconducting system 238

Boron doping

inductively coupled plasma-assisted RF magnetron sputtering deposition of boron-doped microcrystalline Si films 166

Bound magnetic polaron model

CBD

effect of electron irradiation on properties of chemically deposited ${\rm TiO}_2$ nanorods 63

Cellular materials

- the manufacture of spherical salt beads and their use as dissolvable templates for the production of cellular solids via a powder metallurgy route 43
- Ceramic composite
- ultrafine $Al_2O_3-B_4C$ composites consolidated by pulsed electric current sintering 200

Ceramics

the effect of B site doping on infrared emissivity of lanthanum manganites La_{0.8}Sr_{0.2}Mn_{1-x}B_xO₃ (B = Ti or Cu) 212

dielectric and relaxor behavior of BaBi₄Ti₄O₁₅ ceramics 221

compressive property and energy absorption characteristic of open-cell SiCp/AlSi₉Mg composite foams 227

Characterization

effect of melting time on the superconductivity in ${\rm Bi}_{1.7}{\rm Pb}_{0.3}{\rm Sr}_2{\rm CaCu}_2{\rm O}_8$ superconducting system 238

Chemical synthesis

- porous and superparamagnetic magnesium ferrite film fabricated via a precursor route 30
- structural, optical and microscopic studies of tungsten substituted molybdenum diselenide thin films 187
- synthesis, thermal stability, and photocatalytic activity of nanocrystalline gallium nitride via the reaction of Ga₂O₃ and NH₄Cl at low temperature 269

Cobalt magnesium ferrite

synthesis and characterization of novel conductive and magnetic nanocomposites 98

- Co-based Heusler alloys
 - powder neutron diffraction studies for the $L2_1$ phase of Co_2YGa (Y = Ti, V, Cr, Mn and Fe) Heusler alloys 1

Co-doped with Al and Sb

annealing effects of co-doping with Al and Sb on structure and opticalelectrical properties of the ZnO thin films 265

Combined substitution

the effect of the combined substitution of $\rm NH_4^+$ and $\rm CI^-$ on the structure of $\rm [Cs_{0.8}(\rm NH_4)_{0.2}]_2 TeBr_{5.6}Cl_{0.4}$ powder ~L5

Composite materials

compressive property and energy absorption characteristic of open-cell SiCp/AlSi₉Mg composite foams 227

Co-Ni-Ga

- refinement of the γ phase with melt undercooling in a two-phase Co₂NiGa magnetic shape memory alloy 39
- microstructure, transformation temperatures, hardness and magnetic properties of $Co_{36,4+x}Ni_{33,3-x}Ga_{30,3}$ ferromagnetic SMA 183

Core-shell

synthesis and characterization of novel conductive and magnetic nanocomposites 98

Critical temperature

- first-principles study of the ternary semiconductor alloys (Ga,Al)(As,Sb) 80
- Crystal and ligand fields

EPR and optical absorption studies of Cu²⁺ ions doped magnesium citrate decahydrate single crystals 17

Crystal growth

- EPR and optical absorption studies of Cu²⁺ ions doped magnesium citrate decahydrate single crystals 17
- a new low-loss dielectric using CaTiO₃-modified (Mg_{0.95}Mn_{0.05})TiO₃ ceramics for microwave applications 48

Crystal structure

influence of doping elements (Y and Fe) on crystal structure and electrical resistivity of the RNi₂ (R = Gd, Er) compounds 135

Crystallite size

effect of pH on ZnO nanoparticle properties synthesized by sol-gel centrifugation 231

room-temperature ferromagnetism in Ti_{1-x}V_xO₂ nanocrystals synthesized from an organic-free and water-soluble precursor 160

Degree of long range order FeA1 powder neutron diffraction studies for the $L2_1$ phase of Co₂YGa (Y = Ti, V, Cr, Mn and Fe) Heusler alloys 1 DFT Ferroelectricity first-principles study of the ternary semiconductor alloys (Ga,Al)(As,Sb) 80 Dielectric function first-principles study of the ternary semiconductor alloys (Ga,Al)(As,Sb) 80 **Dielectric properties** BiScO₃-modified (K_{0.475}Na_{0.475}Li_{0.05})(Nb_{0.95}Sb_{0.05})O₃ lead-free piezoelectric ceramics L1 Ferromagnetism Sol-gel synthesis and characterization of Ba(1-y)Sr,TiO₃ ceramics 255 Dielectric response a new low-loss dielectric using $CaTiO_3$ -modified ($Mg_{0.95}Mn_{0.05}$)TiO₃ ceramics for microwave applications 48 FP-I APW dielectric and relaxor behavior of BaBi₄Ti₄O₁₅ ceramics 221 Diffusion 80 effect of Cu concentration, solder volume, and temperature on the reaction Fullprof between SnAgCu solders and Ni 149 Dilute magnetic semiconductor room-temperature ferromagnetism in Ti_{1-v}V_vO₂ nanocrystals synthesized from an organic-free and water-soluble precursor 160 Gallium nitride Dislocations a new type of (0 0 1) junction observed in a (B2) Fe-Al-Ni-B alloy by TEM in situ straining 176 269 Dye adsorption Galvanizing synthesis and characterization of novel conductive and magnetic nanocomposites 98 $Ga_{2x}In_{2(1-x)}O_3$ film Dynamic restoration processes the effect of Cu addition on the hot deformation behavior of NiTi shape memory alloys 57 Grain size Elastic properties high pressure phase-transition, elastic and thermal properties of uranium Growth mechanism chalcogenides: A model study 90 Elasticity elastic properties and electronic structures of 4d- and 5d-transition metal mononitrides 243 Hardness **Electrical properties** influence of doping elements (Y and Fe) on crystal structure and electrical resistivity of the RNi₂ (R = Gd, Er) compounds 135 Heusler alloy Electron irradiation effect of electron irradiation on properties of chemically deposited TiO₂ nanorods 63 HgTe Electron paramagnetic resonance EPR and optical absorption studies of Cu²⁺ ions doped magnesium citrate decahydrate single crystals 17 Electronic properties elastic properties and electronic structures of 4d- and 5d-transition metal mononitrides 243 Electronic structure the influence of B variation on the electronic properties of Al₃Ni₂₀B_v 11 Hot deformation Energy transfer role of PbO substitution by Bi₂O₃ on 1.47 µm luminescence properties of Tm³⁺/Tb³⁺-doped Bi₂O₃-GeO₂-Ga₂O₃ glass 126 Equation of state Hot spot high pressure phase-transition, elastic and thermal properties of uranium chalcogenides: A model study 90 Er123 Hydrogen storage influence of hot-spot temperature on oxygen sensing response behavior of Er123 ceramic rods with hot spot 206 Excess oxygen and melting operation effect of melting time on the superconductivity in Bi₁₇Pb₀₃Sr₂CaCu₂O₈ superconducting system 238 Exchange coupling Hvdrothermal magnetic properties of Fe-Co ferromagnetic layers and Fe-Mn/Fe-Co

bilayers obtained by thermo-ionic vacuum arc 23

- a new type of (001) junction observed in a (B2) Fe-Al-Ni-B alloy by TEM in situ straining 176
- BiScO₃-modified (K_{0.475}Na_{0.475}Li_{0.05})(Nb_{0.95}Sb_{0.05})O₃ lead-free piezoelectric ceramics L1

Ferromagnetic shape memory alloy

- microstructure, transformation temperatures, hardness and magnetic properties of Co_{36,4+x}Ni_{33,3-x}Ga_{30,3} ferromagnetic SMA 183
- the magnetic properties of La doped and codoped BiFeO₃ 108
- room-temperature ferromagnetism in Ti_{1-x}V_xO₂ nanocrystals synthesized from an organic-free and water-soluble precursor 160
- first-principles study of the ternary semiconductor alloys (Ga,Al)(As,Sb)
- the effect of the combined substitution of NH₄⁺ and Cl⁻ on the structure of $[Cs_{0.8}(NH_4)_{0.2}]_2$ TeBr_{5.6}Cl_{0.4} powder L5
- synthesis, thermal stability, and photocatalytic activity of nanocrystalline gallium nitride via the reaction of Ga2O3 and NH4Cl at low temperature
- the Zn-rich corner of the Zn-Al-Ti system at 723 K 194
- preparation and characterization of $Ga_{2x}In_{2(1-x)}O_3$ films deposited on ZrO₂(100) substrates by MOCVD 75
- low-field magnetoresistance of La0,7Ca0,3MnO3 perovskite synthesized by reactive milling method 131

- effect of pH on ZnO nanoparticle properties synthesized by sol-gel centrifugation 231
- effects of cerium content on wettability, microstructure and mechanical properties of Sn-Ag-Ce solder alloys 154
- magneto-thermal and magneto-transport behavior around the martensitic transition in $Ni_{50-x}Co_xMn_{40}Sb_{10}$ (x = 9, 9.5) Heusler alloys 140
- solution-chemical syntheses of nanostructure HgTe via a simple hydrothermal process 121
- High pressure phase transition

high pressure phase-transition, elastic and thermal properties of uranium chalcogenides: A model study 90

- High-temperature microstructure
 - high-temperature microstructural characteristics of a novel biomedical titanium alloy 171

- the effect of Cu addition on the hot deformation behavior of NiTi shape memory alloys 57
- influence of hot-spot temperature on oxygen sensing response behavior of Er123 ceramic rods with hot spot 206
- effect of TiH₂ and Mg₂Ni additives on the hydrogen storage properties of magnesium hydride 35

Hydrogen storage materials

towards Y(NH₂BH₃)₃: Probing hydrogen storage properties of YX₃/MNH₂BH₃ (X = F, Cl; M = Li, Na) and YH_{x-3}/NH_3BH_3 composites 144

solution-chemical syntheses of nanostructure HgTe via a simple hydrothermal process 121

Magnetocrystalline anisotropy

In-situ hydrothermal synthesis of three-dimensional MnO₂-CNT nanocomposites and their electrochemical properties 259

- Impedance spectroscopy
- dielectric and relaxor behavior of BaBi₄Ti₄O₁₅ ceramics 221 Inductively coupled plasmas

inductively coupled plasma-assisted RF magnetron sputtering deposition of boron-doped microcrystalline Si films 166

Inorganic materials

porous and superparamagnetic magnesium ferrite film fabricated via a precursor route 30

InSe

structural and optical characterization of single-phase y-In₂Se₃ films with room-temperature photoluminescence 104

In-situ

In-situ hydrothermal synthesis of three-dimensional MnO2-CNT nanocomposites and their electrochemical properties 259

Intermetallics

- the influence of B variation on the electronic properties of Al₂Ni₂₀B₄ 11 effect of Cu concentration, solder volume, and temperature on the reaction between SnAgCu solders and Ni 149
 - a new type of (0 0 1) junction observed in a (B2) Fe-Al-Ni-B alloy by TEM in situ straining 176

IR spectroscopy

the effect of the combined substitution of NH₄⁺ and Cl⁻ on the structure of $[Cs_{0.8}(NH_4)_{0.2}]_2$ TeBr_{5.6}Cl_{0.4} powder L5

L2, phase

powder neutron diffraction studies for the $L2_1$ phase of Co₂YGa (Y = Ti, V, Cr, Mn and Fe) Heusler alloys 1

Lead-free ceramics

 $BiScO_3\text{-}modified \ (K_{0.475}Na_{0.475}Li_{0.05})(Nb_{0.95}Sb_{0.05})O_3 \ lead-free \ piezoelectric$ ceramics L1

Light absorption and reflection

the effect of B site doping on infrared emissivity of lanthanum manganites $La_{0.8}Sr_{0.2}Mn_{1-x}B_xO_3$ (B = Ti or Cu) 212

Low-field magnetoresistance

low-field magnetoresistance of La00.7Ca0.3MnO3 perovskite synthesized by reactive milling method 131

Luminescence

a novel red-emitting phosphor for white light-emitting diodes 53

1.47 µm luminescence

- role of PbO substitution by Bi₂O₃ on 1.47 µm luminescence properties of Tm³⁺/Tb³⁺-doped Bi₂O₃-GeO₂-Ga₂O₃ glass 126
- Magnesium hydride
 - effect of TiH₂ and Mg₂Ni additives on the hydrogen storage properties of magnesium hydride 35

Magnetic and electrical properties

- synthesis and characterization of novel conductive and magnetic nanocomposites 98
- Magnetic films and multi-layers
 - magnetic properties of Fe-Co ferromagnetic layers and Fe-Mn/Fe-Co bilayers obtained by thermo-ionic vacuum arc 23
 - porous and superparamagnetic magnesium ferrite film fabricated via a precursor route 30

Magnetic moment

powder neutron diffraction studies for the $L2_1$ phase of Co₂YGa (Y = Ti, V, Cr, Mn and Fe) Heusler alloys 1

Magnetic shape memory alloy

refinement of the γ phase with melt undercooling in a two-phase Co₂NiGa magnetic shape memory alloy 39

Magnetocaloric effect

the study of the magnetic and room-temperature magnetocaloric properties in spin-reorientation Nd_{1-v}Dy_vCo₄Al (x = 0, 0.1) alloys 7

magneto-thermal and magneto-transport behavior around the martensitic transition in Ni_{50-x}Co_xMn₄₀Sb₁₀ (x = 9, 9.5) Heusler alloys 140

Magnetoresistance magneto-thermal and magneto-transport behavior around the martensitic transition in Ni_{50-x}Co_xMn₄₀Sb₁₀ (x = 9, 9.5) Heusler alloys 140 Manganite low-field magnetoresistance of La_{0.7}Ca_{0.3}MnO₃ perovskite synthesized by reactive milling method 131 Martensitic transformation microstructure, transformation temperatures, hardness and magnetic properties of Co_{36.4+x}Ni_{33.3-x}Ga_{30.3} ferromagnetic SMA 183 Martensitic transition magneto-thermal and magneto-transport behavior around the martensitic transition in $Ni_{50-x}Co_xMn_{40}Sb_{10}$ (x = 9, 9.5) Heusler alloys 140 Mechanical properties the manufacture of spherical salt beads and their use as dissolvable templates for the production of cellular solids via a powder metallurgy route 43 a new type of (0 0 1) junction observed in a (B2) Fe–Al–Ni–B alloy by TEM in

the study of the magnetic and room-temperature magnetocaloric properties

in spin-reorientation $Nd_{1-x}Dy_xCo_4Al(x = 0, 0.1)$ alloys 7

- situ straining 176
- compressive property and energy absorption characteristic of open-cell SiCp/AlSi9Mg composite foams 227
- effect of differential speed rolling on the anisotropy of mechanical properties and texture evolution of AZ31 Mg alloys 273

Metals and alloys

- the manufacture of spherical salt beads and their use as dissolvable templates for the production of cellular solids via a powder metallurgy route 43
- effect of differential speed rolling on the anisotropy of mechanical properties and texture evolution of AZ31 Mg alloys 273

Mg₂Ge

thermodynamic properties of Mg₂Si and Mg₂Ge investigated by first principles method 68

Mg₂Si

- thermodynamic properties of Mg₂Si and Mg₂Ge investigated by first principles method 68
- Microcrystalline silicon
 - inductively coupled plasma-assisted RF magnetron sputtering deposition of boron-doped microcrystalline Si films 166
- Microstructure
 - porous and superparamagnetic magnesium ferrite film fabricated via a precursor route 30
 - the manufacture of spherical salt beads and their use as dissolvable templates for the production of cellular solids via a powder metallurgy route 43
 - effects of cerium content on wettability, microstructure and mechanical properties of Sn-Ag-Ce solder alloys 154
 - ultrafine Al₂O₃-B₄C composites consolidated by pulsed electric current sintering 200

dielectric and relaxor behavior of BaBi₄Ti₄O₁₅ ceramics 221

- Sol-gel synthesis and characterization of Ba_(1-x)Sr_xTiO₃ ceramics 255 MnO₂-CNT nanocomposite
 - In-situ hydrothermal synthesis of three-dimensional MnO2-CNT nanocomposites and their electrochemical properties 259

MOCVD

- preparation and characterization of $Ga_{2x}In_{2(1-x)}O_3$ films deposited on ZrO_2 (100) substrates by MOCVD 75
- structural and optical characterization of single-phase y-In₂Se₃ films with room-temperature photoluminescence 104

MOKE

magnetic properties of Fe-Co ferromagnetic layers and Fe-Mn/Fe-Co bilayers obtained by thermo-ionic vacuum arc 23

Multiferroic

the magnetic properties of La doped and codoped BiFeO₃ 108

Nano-composite

synthesis and characterization of novel conductive and magnetic nanocomposites 98

Nanomaterials Piezoelectricity a novel red-emitting phosphor for white light-emitting diodes 53 BiScO₃-modified (K_{0.475}Na_{0.475}Li_{0.05})(Nb_{0.95}Sb_{0.05})O₃ lead-free piezoelectric Nanorods ceramics L1 effect of electron irradiation on properties of chemically deposited TiO₂ Polvaniline synthesis and characterization of novel conductive and magnetic nanonanorods 63 Nanostructure composites 98 solution-chemical syntheses of nanostructure HgTe via a simple Powder metallurgy hydrothermal process 121 the manufacture of spherical salt beads and their use as dissolvable Nanotubes templates for the production of cellular solids via a powder metallurgy the mechanochemical stability of hydrogen titanate nanostructures 113 route 43 Neutron powder diffraction Precipitation improved thermoelectric properties of AgSbTe₂ based compounds with powder neutron diffraction studies for the $L2_1$ phase of Co₂YGa (Y = Ti, V, Cr, Mn and Fe) Heusler alloys 1 nanoscale Ag₂Te in situ precipitates 215 Nickel-based aluminides Pulsed electric current sintering the influence of B variation on the electronic properties of $Al_3Ni_{20}B_{y}$ 11 ultrafine $Al_2O_3-B_4C$ composites consolidated by pulsed electric current NiTi allov sintering 200 the effect of Cu addition on the hot deformation behavior of NiTi shape memory alloys 57 Raman NiTiCu alloys the magnetic properties of La doped and codoped BiFeO₂ 108 the effect of Cu addition on the hot deformation behavior of NiTi shape Rare earth alloys and compounds memory alloys 57 influence of doping elements (Y and Fe) on crystal structure and electrical resistivity of the RNi₂ (R = Gd, Er) compounds 135 Octahedral rotation Rare earth element the effect of the combined substitution of NH₄⁺ and Cl⁻ on the structure of effects of cerium content on wettability, microstructure and mechanical [Cs_{0.8}(NH₄)_{0.2}]₂TeBr_{5.6}Cl_{0.4} powder L5 properties of Sn-Ag-Ce solder alloys 154 Optical and electrical properties Rare-earth ions annealing effects of co-doping with Al and Sb on structure and opticalrole of PbO substitution by Bi2O3 on 1.47 µm luminescence properties of electrical properties of the ZnO thin films 265 Tm³⁺/Tb³⁺-doped Bi₂O₃-GeO₂-Ga₂O₃ glass 126 Optical properties Refinement EPR and optical absorption studies of Cu²⁺ ions doped magnesium citrate refinement of the γ phase with melt undercooling in a two-phase Co₂NiGa decahydrate single crystals 17 magnetic shape memory alloy 39 the effect of B site doping on infrared emissivity of lanthanum manganites $La_{0.8}Sr_{0.2}Mn_{1-x}B_xO_3$ (B = Ti or Cu) 212 Semiconductors structural, optical and microscopic studies of tungsten substituted Organic crystals EPR and optical absorption studies of Cu²⁺ ions doped magnesium citrate molybdenum diselenide thin films 187 decahydrate single crystals 17 Silver antimony tellurides improved thermoelectric properties of AgSbTe₂ based compounds with Oxygen sensor influence of hot-spot temperature on oxygen sensing response behavior of nanoscale Ag₂Te in situ precipitates 215 Er123 ceramic rods with hot spot 206 Sintering Oxygen vacancies and interstitials the manufacture of spherical salt beads and their use as dissolvable room-temperature ferromagnetism in $Ti_{1-x}V_xO_2$ nanocrystals synthesized templates for the production of cellular solids via a powder metallurgy from an organic-free and water-soluble precursor 160 route 43 ultrafine Al₂O₃-B₄C composites consolidated by pulsed electric current Particle size sintering 200 effect of pH on ZnO nanoparticle properties synthesized by sol-gel Slack's equation centrifugation 231 thermodynamic properties of Mg₂Si and Mg₂Ge investigated by first Pb-free solder principles method 68 effects of cerium content on wettability, microstructure and mechanical Solar cells inductively coupled plasma-assisted RF magnetron sputtering deposition of properties of Sn-Ag-Ce solder alloys 154 boron-doped microcrystalline Si films 166 pН effect of pH on ZnO nanoparticle properties synthesized by sol-gel Soldering effect of Cu concentration, solder volume, and temperature on the reaction centrifugation 231 Phase diagram between SnAgCu solders and Ni 149 the Zn-rich corner of the Zn-Al-Ti system at 723 K 194 Sol-gel method effect of pH on ZnO nanoparticle properties synthesized by sol-gel Phase transformation high-temperature microstructural characteristics of a novel biomedical centrifugation 231 titanium alloy 171 Sol-gel process Sol-gel synthesis and characterization of Ba_(1-x)Sr_xTiO₃ ceramics 255 Phase transitions elastic properties and electronic structures of 4d- and 5d-transition metal Sol-gel spin-coating method mononitrides 243 annealing effects of co-doping with Al and Sb on structure and optical-Photocatalysis activity electrical properties of the ZnO thin films 265 synthesis, thermal stability, and photocatalytic activity of nanocrystalline Solid-state reaction gallium nitride via the reaction of Ga2O3 and NH4Cl at low temperature a novel red-emitting phosphor for white light-emitting diodes 53 269 the effect of B site doping on infrared emissivity of lanthanum manganites Photoluminescence $La_{0.8}Sr_{0.2}Mn_{1-x}B_xO_3$ (B = Ti or Cu) 212 structural and optical characterization of single-phase γ -In₂Se₃ films with Solid-state reactions dielectric and relaxor behavior of BaBi4Ti4015 ceramics 221 room-temperature photoluminescence 104

Solution-chemical

solution-chemical syntheses of nanostructure HgTe via a simple hydrothermal process 121

Spectroscopic properties

role of PbO substitution by Bi_2O_3 on 1.47 μm luminescence properties of Tm^{3+}/Tb^{3+} -doped $Bi_2O_3-GeO_2-Ga_2O_3$ glass 126

Spin-polarized tunneling

low-field magnetoresistance of La_{0.7}Ca_{0.3}MnO₃ perovskite synthesized by reactive milling method 131

Spin-reorientation

the study of the magnetic and room-temperature magnetocaloric properties in spin-reorientation $Nd_{1-x}Dy_xCo_4Al (x = 0, 0.1)$ alloys 7

Structural phase transitions

- the mechanochemical stability of hydrogen titanate nanostructures 113 Supercapacitor
- *In-situ* hydrothermal synthesis of three-dimensional MnO₂-CNT nanocomposites and their electrochemical properties 259

Synthesis

effect of melting time on the superconductivity in Bi_{1.7}Pb_{0.3}Sr₂CaCu₂O₈ superconducting system 238

TEM

- a new type of (0 0 1) junction observed in a (B2) Fe–Al–Ni–B alloy by TEM *in situ* straining 176
- effect of differential speed rolling on the anisotropy of mechanical properties and texture evolution of AZ31 Mg alloys 273

Tensile strength

effects of cerium content on wettability, microstructure and mechanical properties of Sn–Ag–Ce solder alloys 154

Ternary alloys

- first-principles study of the ternary semiconductor alloys (Ga,Al)(As,Sb) 80 Thermal analysis
- the influence of B variation on the electronic properties of $Al_3Ni_{20}B_x$ 11 Thermal conductivity
- thermodynamic properties of Mg_2Si and Mg_2Ge investigated by first principles method 68

Thermodynamic properties

- the influence of B variation on the electronic properties of $Al_3Ni_{20}B_x$ 11 Thermoelectric materials
- improved thermoelectric properties of AgSbTe₂ based compounds with nanoscale Ag₂Te *in situ* precipitates 215

Thermoelectric properties

improved thermoelectric properties of AgSbTe₂ based compounds with nanoscale Ag₂Te *in situ* precipitates 215

Thermogravimetric analysis

- synthesis, thermal stability, and photocatalytic activity of nanocrystalline gallium nitride via the reaction of Ga₂O₃ and NH₄Cl at low temperature 269
- Thermophysical properties
 - high pressure phase-transition, elastic and thermal properties of uranium chalcogenides: A model study 90

Thin films

- effect of electron irradiation on properties of chemically deposited ${\rm TiO}_2$ nanorods 63
- structural, optical and microscopic studies of tungsten substituted molybdenum diselenide thin films 187

Three-dimensional nanostructure

In-situ hydrothermal synthesis of three-dimensional MnO₂-CNT nanocomposites and their electrochemical properties 259

TiO₂

effect of electron irradiation on properties of chemically deposited TiO₂ nanorods 63

Titanates

- the mechanochemical stability of hydrogen titanate nanostructures 113 Titanium alloy
 - high-temperature microstructural characteristics of a novel biomedical titanium alloy 171
- $Ti_{1-x}V_xO_2$ nanocrystals

room-temperature ferromagnetism in Ti_{1-x}V_xO₂ nanocrystals synthesized from an organic-free and water-soluble precursor 160

Transition metal alloys and compounds

elastic properties and electronic structures of 4d- and 5d-transition metal mononitrides 243

- Transmission electron microscopey
 - high-temperature microstructural characteristics of a novel biomedical titanium alloy 171
- Transmission electron microscopy

effect of differential speed rolling on the anisotropy of mechanical properties and texture evolution of AZ31 Mg alloys 273

TVA

magnetic properties of Fe–Co ferromagnetic layers and Fe–Mn/Fe–Co bilayers obtained by thermo-ionic vacuum arc 23

Undercooling

refinement of the γ phase with melt undercooling in a two-phase Co₂NiGa magnetic shape memory alloy 39

a novel red-emitting phosphor for white light-emitting diodes 53

Wettability

UV-LEDs

effects of cerium content on wettability, microstructure and mechanical properties of Sn-Ag-Ce solder alloys 154

X-ray diffraction

- structural, optical and microscopic studies of tungsten substituted molybdenum diselenide thin films 187
- synthesis, thermal stability, and photocatalytic activity of nanocrystalline gallium nitride via the reaction of Ga_2O_3 and NH_4Cl at low temperature 269

Yttrium

towards Y(NH₂BH₃)₃: Probing hydrogen storage properties of YX₃/MNH₂BH₃ (X = F, Cl; M = Li, Na) and YH_{y-3}/NH₃BH₃ composites 144

Zn–Al–Ti system

the Zn-rich corner of the Zn-Al-Ti system at 723 K 194

ZnO thin films

annealing effects of co-doping with Al and Sb on structure and opticalelectrical properties of the ZnO thin films 265

Zn-rich corner

the Zn-rich corner of the Zn-Al-Ti system at 723 K 194

ZrO₂ substrate

preparation and characterization of $Ga_{2x}In_{2(1-x)}O_3$ films deposited on $ZrO_2(1 \ 0 \ 0)$ substrates by MOCVD 75